Nearly Isotropic Upper Critical Field in Pressurized Trilayer Nickelate $La_4Ni_3O_{10-\delta}$

Di Peng,[1,2,*] Yaolong Bian,[3,4,*] Zhenfang Xing,[2,*] Lixing Chen,[5,*] Jiaqiang Cai,[3,4] Tao Luo,[2] Fujun Lan,[2] Yuxin Liu,[2] Yinghao Zhu,[5] Enkang Zhang,[5] Zhaosheng Wang,[3] Yuping Sun,[3] Yuzhu Wang,[6] Xingya Wang,[6] Chenyue Wang,[6] Yuqi Yang,[7] Yanping Yang,[2] Hongliang Dong,[2] Hongbo Lou,[2] Zhidan Zeng,[2] Zhi Zeng,[8] Mingliang Tian,[3] Jun Zhao,[5,9,†] Qiaoshi Zeng,[1,2,‡] Jinglei Zhang,[3,§] and Ho-kwang Mao[1,2]

[1]*Shanghai Key Laboratory of Material Frontiers Research in Extreme Environments (MFree), Shanghai Advanced Research in Physical Sciences (SHARPS), Shanghai, China*
[2]*Center for High Pressure Science and Technology Advanced Research, Shanghai, China*
[3]*Anhui Key Laboratory of Low-Energy Quantum Materials and Devices, High Magnetic Field Laboratory (CHMFL), Hefei Institutes of Physical Science, Chinese Academy of Sciences, Hefei, China*
[4]*Science Island Branch of Graduate School, University of Science and Technology of China, Hefei, China*
[5]*State Key Laboratory of Surface Physics and Department of Physics, Fudan University, Shanghai, China*
[6]*Shanghai Synchrotron Radiation Facility, Shanghai Advanced Research Institute, Chinese Academy of Sciences, Shanghai, China*
[7]*Human Institute, ShanghaiTech University, Shanghai, China*
[8]*Key Laboratory of Materials Physics, Anhui Key Laboratory of Nanomaterials and Nanotechnology, Institute of Solid State Physics, HFIPS, Chinese Academy of Sciences, Hefei, China*
[9]*Institute of Nanoelectronics and Quantum Computing, Fudan University, Shanghai, China*

(Received 12 August 2025; revised 14 January 2026; accepted 16 March 2026; published 8 April 2026)

Evidence of superconductivity has recently been reported in pressurized nickelates, providing a new platform to explore high-temperature superconductivity. However, detailed experimental characterization of the superconducting properties of nickelates under pressure remains limited and technically challenging. Here, we report the first full temperature-dependent measurements of the upper critical field ($\mu_0 H_{c2}$) in pressurized trilayer nickelate $La_4Ni_3O_{10-\delta}$ single crystal, achieved by integrating advanced high-magnetic-field and high-pressure techniques. Remarkably, $La_4Ni_3O_{10-\delta}$ exhibits nearly isotropic superconductivity, with the anisotropic parameter γ decreasing monotonically from 1.4 near T_c to 1 at lower temperatures. By applying a two-band model analysis out of plane and in plane $\mu_0 H_{c2}$, we uncover a compensation of anisotropic diffusivity between bands primarily originating from d_{z^2} and $d_{x^2-y^2}$ orbitals, resulting in an exceptionally isotropic superconducting characteristic. These findings indicate the significant contribution of the d_{z^2} orbital to superconductivity in pressurized $La_4Ni_3O_{10-\delta}$ and provide essential constraints for theoretical models of the pairing mechanism in Ruddlesden-Popper nickelates.

DOI: 10.1103/h5sv-dzd1 Subject Areas: Superconductivity

I. INTRODUCTION

The recent discovery of superconductivity in Ruddlesden-Popper (RP) nickelates has attracted significant interest [1–7]. An initial result was the observation of superconductivity in the bilayer RP nickelate $La_3Ni_2O_{7-\delta}$ with the critical temperature (T_c) near 80 K at pressures above 14 GPa [1]. Subsequent studies revealed zero-resistance states under hydrostatic pressure [2,3,7]. However, the superconducting volume fraction for single-crystalline $La_3Ni_2O_{7-\delta}$ remained low [3,8]. Unambiguous bulk superconductivity with the T_c up to 30 K was reported in the single crystal of trilayer RP nickelate $La_4Ni_3O_{10-\delta}$ under pressure [4–6]. More recently, superconductivity was reported in bilayer nickelate ultrathin films with substrate confinement [9–11]. Both $La_3Ni_2O_{7-\delta}$ and $La_4Ni_3O_{10-\delta}$ host a quasi-two-dimensional (2D) crystal structure, with an approximate unit cell comprising NiO_2 layers that is isostructural with the CuO_2 plane in the superconducting cuprates [1,5]. However, the presence of apical oxygens in RP nickelates leads to unique electronic configurations ($d^{7.5}$ for $La_3Ni_2O_{7-\delta}$ and $d^{7.33}$ for $La_4Ni_3O_{10-\delta}$), which are different from the $3d^9$ configuration in cuprates [1,5,12]. Theoretical studies suggest that

*These authors contributed equally to this work.
†Contact author: zhaoj@fudan.edu.cn
‡Contact author: zengqs@hpstar.ac.cn
§Contact author: zhangjinglei@hmfl.ac.cn

interlayer coupling involving Ni $3d_{z^2}$ and apical O p orbitals, high-pressure-induced partial occupation of the $3d_{x^2-y^2}$ orbital (as in cuprates), or a combination of both could be essential for superconducting pairing. These scenarios have fueled debate over the respective roles of the d_{z^2} and $d_{x^2-y^2}$ orbitals in the pairing mechanism. Current models broadly split into two groups: one attributing superconductivity primarily to d_{z^2} orbitals [13–29]; the other emphasizing the contribution of $d_{x^2-y^2}$ orbitals [12,30–40] leading to a variety of proposed pairing symmetries, including s-wave [13,16–19,23,27,32,41–49], d-wave [30,31], and more complex forms [24,36,45,50–55]. To resolve this issue, experimental investigations, particularly those capable of directly probing the superconducting properties of RP nickelates under high pressure, are urgently needed.

The upper critical field ($\mu_0 H_{c2}$) is a fundamental characteristic of a superconductor, essential for elucidating pairing mechanisms and assessing application potential. In cuprate high-temperature superconductors, $\mu_0 H_{c2}$ is highly anisotropic, which reflects the 2D nature of their crystal and electronic pairing associated with the 2D $d_{x^2-y^2}$ orbitals [56,57]. In contrast, the anisotropy of $\mu_0 H_{c2}$ in most iron-based superconductors is weaker than that of cuprates, owing to a more three-dimensional (3D) electronic structure and multiband effects [58,59]. It is therefore both timely and important to directly determine $\mu_0 H_{c2}$ and its anisotropy for RP nickelate superconductors. However, due to the necessity of high pressure to induce superconductivity and a high magnetic field to access $\mu_0 H_{c2}(0)$, experimental progress in this direction is markedly hampered. The technical challenge lies in simultaneously achieving hydrostatic pressures exceeding 50 GPa and steady magnetic fields exceeding 30 T, while maintaining cryogenic conditions. The bulky dimensions of conventional pressure cells restrict modifications to crystal axis orientations under high pressures, which are essential for conducting anisotropy measurements.

In this study, we overcome these technical challenges by designing a specialized diamond anvil cell (DAC), which enables direct measurements of electrical resistivity in single-crystal $La_4Ni_3O_{10-\delta}$ under extreme conditions, specifically pressures up to 50.2 GPa and magnetic fields up to 34 T along both out-of-plane ($H \perp ab$) and in-plane ($H \parallel ab$) directions. We establish a comprehensive temperature magnetic-field phase diagram for $La_4Ni_3O_{10-\delta}$, revealing remarkably isotropic upper critical field behavior over the entire temperature range. The anisotropic ratio $\gamma = \mu_0 H_{c2}^{\parallel}/\mu_0 H_{c2}^{\perp}$ monotonically decreases from 1.4 near T_c to 1 at the lowest-measured temperature. The temperature dependence of $\mu_0 H_{c2}(T)$, in both field directions, can be interpreted within the two-band model, allowing us to qualitatively evaluate the

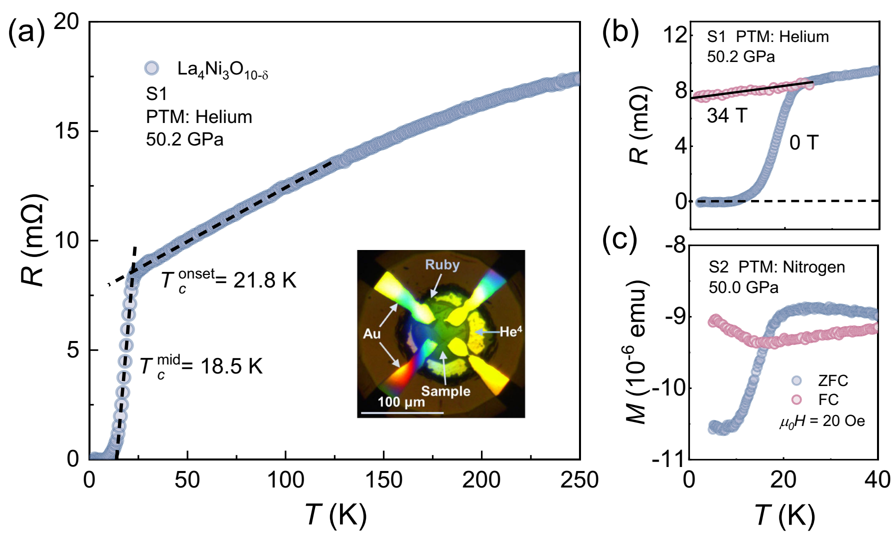

FIG. 1. Superconductivity of $La_4Ni_3O_{10-\delta}$ single crystal under high pressure. (a) Temperature dependence of resistance of $La_4Ni_3O_{10-\delta}$ (sample S1) at 50.2 GPa. The superconducting transition temperature is determined from the resistance with onset at 21.8 K and midpoint at 18.5 K, respectively. The black dashed line demonstrates the linear-T fit of the normal-state resistance. Inset: a photograph of the electrodes used for high-pressure resistance measurements. The lamella was carved from a single crystal by using focused-ion-beam (FIB) milling and mounted with a-b plane parallel to the culet of the DAC. The sample was loaded under helium as the pressure-transmitting medium (PTM). (b) Temperature dependence of the resistance at zero field (blue dots) and high field (34 T, red dots). The data are obtained from sample S1. The zero-field data display a magnified view of the low-temperature region presented in Fig. 1(a). The high-field data are extracted from the resistance-magnetic-field (R-H) curve [Fig. 2(a)]. The black dashed line is a guide for T-linear resistance to the lowest temperature. (c) The raw data of the dc magnetization for $La_4Ni_3O_{10-\delta}$ (sample S2) under a pressure of 50.0 GPa [5]. Magnetization measurements were performed in the nitrogen DAC, with a magnetic field of 20 Oe applied perpendicular to the a-b plane. A clear superconducting diamagnetic response is clearly observed in the zero-field-cooled (ZFC) curve.

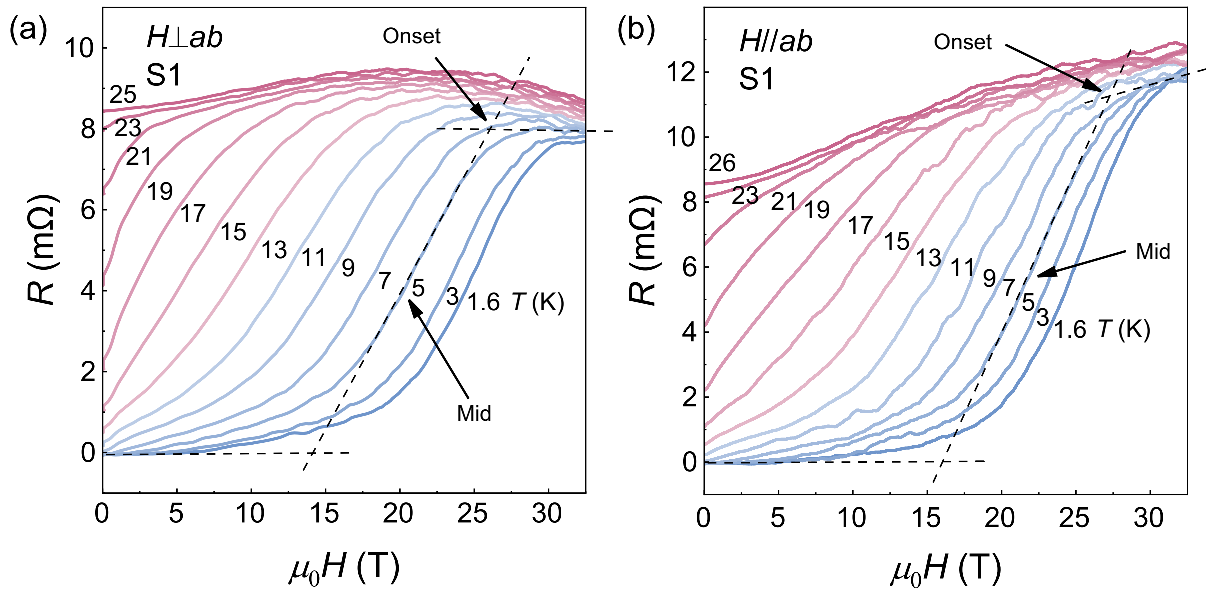

FIG. 2. Magnetic-field dependence of the resistance of $La_4Ni_3O_{10-\delta}$ single crystal at 50.2 GPa. (a),(b) Magnetic-field dependence of resistance at different temperatures with $\mathbf{H} \perp ab$ (a) and $\mathbf{H} \parallel ab$ (b). The superconducting transition shifts to a lower magnetic field as temperature increases. The magnetoresistance effect is weak for $\mathbf{H} \perp ab$, while it is pronounced in the case of $\mathbf{H} \parallel ab$. As a consequence, in the presence of an in-plane magnetic field, the SC transition becomes significantly broadened at higher temperatures.

diffusivity of each band. Our analysis further demonstrates that the d_{z^2} and $d_{x^2-y^2}$ bands have opposing anisotropies, leading to such isotropic superconductivity in $La_4Ni_3O_{10-\delta}$.

II. RESULTS

A. Bulk superconductor properties and structural characterizations

We first focus on the superconductivity of single-crystal $La_4Ni_3O_{10-\delta}$ at zero field. The electrical resistance measurements under pressure were performed using a homemade DAC. Helium was employed as the pressure-transmitting medium to guarantee the best hydrostaticity in the DAC. As shown in the inset of Fig. 1, the sample was loaded with the *a*-*b* plane, which is the cleavage plane of a $La_4Ni_3O_{10-\delta}$ single crystal, parallel to the diamond anvil culet of the DAC. Synchrotron x-ray single-crystal diffraction measurements demonstrate that the sample we studied maintains its single-crystal structure feature up to 50.2 GPa (see Supplemental Material Fig. S1 [60]). Figure 1(a) displays the resistance as a function of temperature at 50.2 GPa. A clear superconducting transition is observed in resistance, with an onset at 21.8 K and a midpoint at 18.5 K, respectively. To verify bulk superconductivity, direct current (dc) magnetic susceptibility was measured on sample S2 from the same batch. The bulk T_c ($T_c^{\mathrm{onset}} = 18.6$ and $T_c^{\mathrm{mid}} = 14.9$ K) determined from the magnetic susceptibility is slightly lower than that determined from the resistance. The estimated superconducting volume fraction of our sample is approximately 86% [5]. The normal-state resistance follows a linear temperature dependence up to approximately 125 K, indicative of strange-metal behavior. Such characteristics have been widely observed in optimally doped cuprates [61,62], certain iron-based superconductors [63,64], and nickelate-based superconductors [2,5,65]. Most importantly, when superconductivity is completely suppressed by a magnetic field of 34 T, the T-linear resistance persists to the lowest-measured temperature, implying the presence of a pressure-induced quantum critical point in $La_4Ni_3O_{10-\delta}$.

B. *In situ* transport measurements under high pressure and high magnetic field

Figures 2(a) and 2(b) display the magnetic-field dependence of the electrical resistance for $La_4Ni_3O_{10-\delta}$ single crystals. In order to estimate the anisotropy of the superconductivity, the measurements were conducted with the magnetic field applied along the out-of-plane [Fig. 2(a)] and in-plane [Fig. 2(b)] directions. The superconducting transition gradually shifted to a lower magnetic field with increasing temperature. In the presence of an in-plane magnetic field, the superconducting (SC) transition broadens significantly at higher temperatures. We noticed that such a broadening behavior is not observed in the R-T curve under a magnetic field (see Supplemental Material Fig. S3 [60]). Thus, it is likely attributed to a magnetoresistance effect, as we discuss below, instead of thermally activated flux flow in the vortex state as reported in $La_3Ni_2O_{7-\delta}$ [2,3]. Above T_c, the magnetoresistance (MR) of $La_4Ni_3O_{10-\delta}$ displays distinct field-orientation dependence. Specifically, the out-of-plane MR is quite small and exhibits a weak "humplike" feature, whereas a

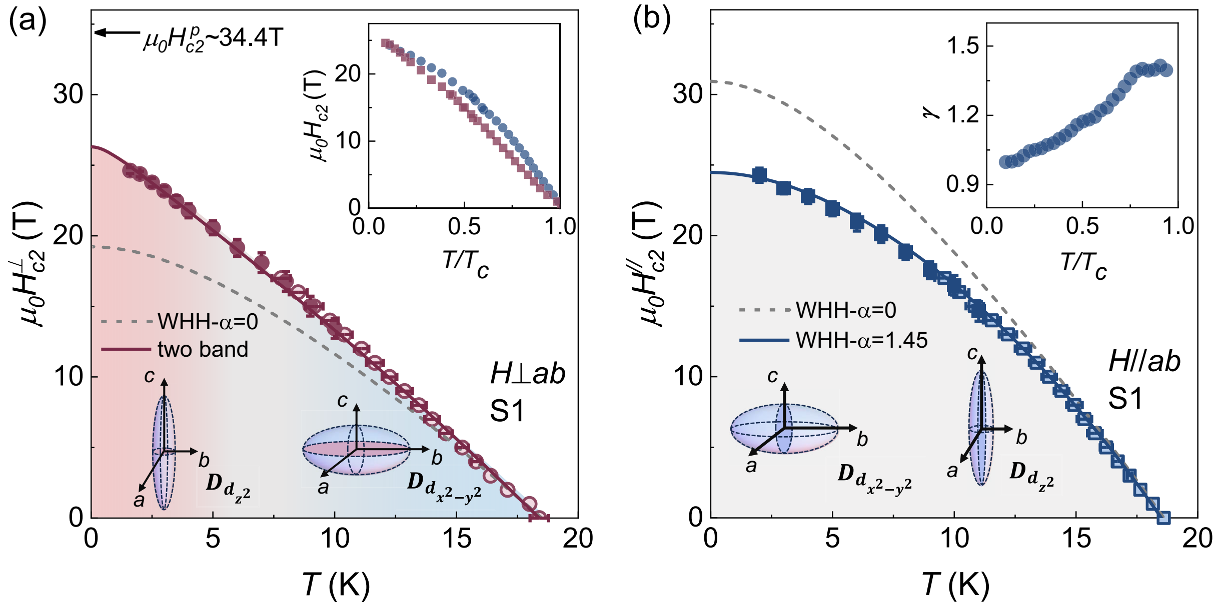

FIG. 3. The upper critical field μ_0H_{c2} of $La_4Ni_3O_{10-\delta}$ single crystal at 50.2 GPa. (a),(b) μ_0H_{c2}-T phase diagrams for magnetic fields along the c axis (a) and in the a-b plane (b). Solid circles (•) and squares (■) are obtained from the R-H curves [Figs. 2(a) and 2(b)]. Open circles (∘) and squares (□) are taken from R-T curves (see Supplemental Material Fig. S3 [60]). To minimize the effects of magnetoresistance and superconducting fluctuations, the values of μ_0H_{c2} and T_c are determined from the midpoint of the superconducting transitions. The method for error determination is illustrated in Supplemental Material Fig. S4 [60]. The blue solid line and the gray dashed line correspond to the WHH theory calculated with and without the spin-paramagnetic effect, respectively. The red solid line represents the best fit of the two-band model in the case of strong-interband coupling with $\lambda_{11} = \lambda_{22} = 0.2$ and $\lambda_{12} = \lambda_{21} = 0.7$. The schematic diagrams illustrate the diffusivity of the bands primarily originating from d_{z^2} and $d_{x^2-y^2}$ orbitals. The red and blue regions represent the behavior of $\mu_0H_{c2}^{\perp}(T)$ is determined by $D_{d_{x^2-y^2}}$ and $D_{d_{z^2}}$, respectively. The inset of (a) overlays the μ_0H_{c2} data for both field orientations. The inset of (b) shows the corresponding temperature dependence of the anisotropic parameter $\gamma = \mu_0H_{c2}^{\parallel}/\mu_0H_{c2}^{\perp}$.

more pronounced positive MR is observed for $H \parallel ab$. Further investigation is required to clarify the origin of this anisotropic MR in the normal state.

C. Analysis of the upper critical field and its anisotropy

Figure 3 illustrates the upper critical fields as a function of temperature for magnetic fields applied perpendicular $[\mu_0H_{c2}^{\perp}(T)]$ and parallel $[\mu_0H_{c2}^{\parallel}(T)]$ to the a-b plane. To minimize the effects of magnetoresistance and superconducting fluctuations, the critical fields and critical temperatures are determined from the midpoint of the superconducting transitions. The $\mu_0H_{c2}^{\perp}(T)$ increases linearly with decreasing temperature. On the contrary, the $\mu_0H_{c2}^{\parallel}(T)$ shows a convex curvature. The upper critical field reaches approximately 24.4 T at the lowest temperature for both field orientations. The estimated coherence length $[\xi_{\parallel}(1.8\ \mathrm{K}) \approx \xi_{\perp}(1.8\ \mathrm{K}) = 33\ \text{Å}]$ is an order of magnitude larger than the thickness of the superconducting NiO_2 layers (approximately 3.7 Å) [5], demonstrating the 3D nature of the superconductivity. Notably, the nearly isotropic upper critical field can extend across the entire temperature range, as evidenced by the fact that the anisotropic ratio $\gamma = \mu_0H_{c2}^{\parallel}/\mu_0H_{c2}^{\perp}$ varies only from 1 (at base temperature) to 1.4 (at near T_c). The results are reproducibly observed on another sample (sample S4, see Supplemental Material Figs. S6–S9 [60]).

In a superconductor, the Cooper pairs can be destroyed by a magnetic field through two primary mechanisms: (i) The orbital pair breaking due to the Lorentz force acting via the charge on the paired electrons, known as the orbital limit [66]. The orbital-limited upper critical field $\mu_0H_{c2}^{\mathrm{orb}}(0)$ for a single-band BCS superconductor is determined by the initial slope of μ_0H_{c2} at T_c, i.e., $\mu_0H_{c2}^{\mathrm{orb}}(0) = -0.69T_c[(dH_{c2})/(dT)]_{|T=T_c}$. (ii) The Pauli paramagnetic pair breaking as a result of the Zeeman effect, which aligns the spins of two electrons with the applied field [67]. The Pauli paramagnetic limiting field for weakly coupled BCS superconductors is given by $\mu_0H_{c2}^{p}(0) = 1.86T_c$, which is usually field-orientation independent. In our case, the initial slope of μ_0H_{c2} at T_c is determined as 1.5 and 2.5 T/K for $H \perp ab$ and $H \parallel ab$, respectively. The derived out-of-plane and in-plane $\mu_0H_{c2}^{\mathrm{orb}}(0)$ are 19.1 and 31.9 T, respectively, both of which are below the Pauli limit of 34.4 T. To comprehensively

TABLE I. The derived parameters for $La_4Ni_3O_{10-\delta}$.

	$\mu_0 H_{c2}$ (1.8 K) (T)	$\mu_0 H_{c2}^{orb}(0)$ (T)	$\mu_0 H_{c2}^{p}(0)$ (T)	D_1 (cm^2/ sec)	D_2 (cm^2/ sec)
$H \perp ab$	24.4	19.1	34.4	$D_1^{ab} = 1.2$	$D_2^{ab} = 0.1$
$H \parallel ab$	24.4	31.9	34.4	$D_1^{c} = 0.65$	$D_2^{c} = 7.7$

evaluate the spin-paramagnetic and orbital pair-breaking effects, we fitted the experimental data of $\mu_0 H_{c2}(T)$ with the Werthamer-Helfand-Hohenberg (WHH) model [66]. The fitting parameters of α (Maki parameter) and λ_{so} are defined by $\alpha = \sqrt{2}\{[\mu_0 H_{c2}^{orb}(0)]/[\mu_0 H^p(0)]\}$ and $\lambda_{so} = [1/(3\pi T_c \tau_2)]$, where $1/\tau_2$ reflects the spin-orbit scattering rate. As shown in Fig. 3, by adjusting the values of α and λ_{so}, $\mu_0 H_{c2}^{\parallel}(T)$ can be well described by the WHH model with the small value of $\alpha = 1.45$ and $\lambda_{so} = 1.08$. However, the experimental data for $\mu_0 H_{c2}^{\perp}(T)$ lie above the theoretical curve even with spin effects neglected ($\alpha = 0$, $\lambda_{so} = 0$). Our analysis indicates that the orbital effect is the dominant pair-breaking mechanism for $La_4Ni_3O_{10-\delta}$. Thus, the scenario of isotropic Pauli-limited superconductivity, as proposed for infinite-layer nickelates [68–70], is unlikely to apply to the isotropic upper critical field of $La_4Ni_3O_{10-\delta}$.

Previous theoretical studies have predicted that superconductivity in pressurized RP nickelates may emerge in several disconnected regions of the Fermi surface [12,46]. Here, we utilize a two-band model to describe the upper critical field of $La_4Ni_3O_{10-\delta}$ [71]. The details of the parameters in the two-band theory are outlined in Supplemental Material [60]. We first focus on the coupling constant λ_{nm}, emphasizing two scenarios: strong-intraband coupling ($\lambda_{12}\lambda_{21} \ll \lambda_{11}\lambda_{22}$) and strong-interband coupling ($\lambda_{12}\lambda_{21} \gg \lambda_{11}\lambda_{22}$). The former was discussed in dirty MgB_2 [71], while the latter is relevant to some iron-based SCs [72]. When the magnetic field is applied in the out-of-plane direction, the fittings in these two cases exhibit a significant difference. The possibility of strong-intraband coupling can be ruled out in $La_4Ni_3O_{10-\delta}$, as the calculated $\mu_0 H_{c2}^{\perp}(T)$ with $\lambda_{12}\lambda_{21} \ll \lambda_{11}\lambda_{22}$ exhibits a strong-upturn feature at low temperatures that deviates from the measured data (see Supplemental Material Fig. S10 [60]). The discussions in the main text [represented by the solid line in Fig. 3(a)] are based on strong-interband coupling ($\lambda_{11} = \lambda_{22} = 0.2$ and $\lambda_{12} = \lambda_{21} = 0.7$), which emphasizes the importance of the strong-interband coupling for superconductivity in RP nickelates.

Now, we turn to D_1 and D_2, the diffusivity of each band. The upper critical field near T_c is mainly governed by the band with the higher diffusivity D_1, which can be deduced from $(8\phi_0 k_B)/[\pi^2(dH_{c2}/dT)_{|T=T_c}]$, while the band with the lower diffusivity D_2 dominates the low-temperature behavior of $\mu_0 H_{c2}(T)$. This two-gap model captures the main features of the $\mu_0 H_{c2}^{\perp}(T)$ curve, yielding $\eta^{\perp} = D_2^{ab}/D_1^{ab} = 0.083$. Notably, under the condition of equal band diffusivities ($D_1 \approx D_2$), the two-band model formally reduces to the single-band de Gennes–Maki formula within the WHH theory. Therefore, when analyzing $\mu_0 H_{c2}^{\parallel}(T)$ within the two-band framework, it is reasonable to assume that the anisotropy parameter satisfies $\eta^{\parallel} = \sqrt{D_2^{ab} D_2^{c}}/\sqrt{D_1^{ab} D_1^{c}} \approx 1$. Our fitting results are listed in Table I, which further reveals that the two bands, in terms of diffusivity, exhibit strong asymmetry; i.e., band 1 has higher a-b-plane diffusivity ($D_1^{ab}/D_1^{c} > 1$) and band 2 is more itinerant along the c axis ($D_2^{ab}/D_2^{c} < 1$). The most plausible orbital assignment consistent with density functional theory calculations [46] is that D_1 predominantly reflects the diffusivity of $d_{x^2-y^2}$ electrons ($D_{d_{x^2-y^2}}$), which are associated with the nearly cylindrical, two-dimensional pockets (α, β_1, and β_2); whereas D_2 may be linked to d_{z^2}

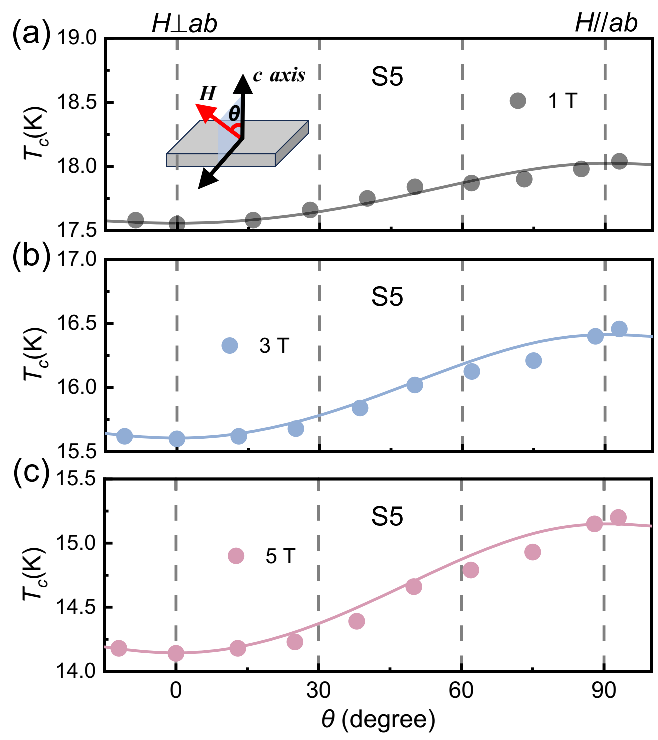

FIG. 4. The angular dependence of the superconducting critical temperature $T_c(\theta)$ at magnetic fields of $\mu_0 H_{c2} = 1$, 3, and 5 T. θ is the angle between the magnetic field and the c axis of the sample. The solid lines show the fittings to Eq. (1). Here, $T_c(\theta)$ is determined from the superconducting midpoint.

electron diffusivity ($D_{d_{z^2}}$), contributing to the other pockets (γ and δ). However, one cannot expect a two-band model to fully describe such a complex band structure for pressurized $La_4Ni_3O_{10-\delta}$. A more definitive determination of its Fermi surface characteristics will require further investigation through additional experimental methods.

D. Angular dependence of the upper critical field

In order to further characterize the nature of the anisotropy of $\mu_0 H_{c2}$, we have measured the angular dependence of the electrical resistivity at various magnetic fields (sample S5, see Supplemental Material Fig. S13 [60]). Figure 4 plots the angular dependence of $T_c(\theta)$, where θ is the angle between the magnetic field and the c axis of the sample as marked in the inset. The angular dependence of the upper critical field in 3D superconductors can be described by the single-band anisotropic Ginzburg-Landau theory [73,74]. In the case where $\mu_0 H_{c2}$ is a linear function of temperature, the angular dependence of $\mu_0 H_{c2}$ can be converted to that of T_c by [75]

$$T_c(\theta) = T_{c0} + H/(\partial H_{c2}^{H//c}/\partial T)\sqrt{\cos^2\theta + \gamma^{-2}\sin^2\theta}, \quad (1)$$

where T_{c0} is the zero-field superconducting transition temperature and H is the applied magnetic field. In our case, the upper critical field near T_c indeed shows nearly linear temperature dependence for both $H \perp ab$ and $H \parallel ab$. Therefore, we can estimate the anisotropic parameter γ from the angular dependence of T_c. As shown in Fig. 4, $T_c(\theta)$ exhibits minima near 0° and maxima near 90°, and its angular dependence is well described by Eq. (1) (solid lines). The above fittings give $\gamma = 2.3$, 1.48, and 1.32 for $\mu_0 H = 1$, 3, and 5 T, respectively. These values of γ are very close to those determined from $\mu_0 H_{c2}^{\parallel}/\mu_0 H_{c2}^{\perp}$ (see Supplemental Material Fig. S14 [60]), which further confirms the nearly isotropic superconductivity in $La_4Ni_3O_{10-\delta}$.

III. DISCUSSION

At ambient pressure, the Fermi surface of RP nickelates is primarily derived from the $d_{x^2-y^2}$ orbital, which bears notable similarities to cuprates [5]. The emergence of superconductivity under pressure is concomitant with the structural transition, raising the key question of whether the d_{z^2} dominant bands intersect the Fermi level. If the electronic structure is mainly characterized by the $d_{x^2-y^2}$ orbital, the upper critical field would typically be highly anisotropic. However, this is not the case for $La_4Ni_3O_{10-\delta}$, in which anisotropy of the $d_{x^2-y^2}$ orbital electrons is compensated by that of the d_{z^2} orbital. The nearly isotropic superconductivity of $La_4Ni_3O_{10-\delta}$ is reminiscent of the behavior observed in optimally doped iron-based superconductors, such as $Ba_{0.6}K_{0.4}Fe_2As_2$, where the anisotropic parameter is approximately 2 near T_c and decreases toward 1 at low temperatures [59]. In the case of iron-based superconductors, interband interactions associated with multiple orbitals also play a significant role. In this sense, our result is compatible with theoretical proposals that highlight the role of both the d_{z^2} and $d_{x^2-y^2}$ bands as essential to the emergence of superconductivity in pressurized $La_4Ni_3O_{10-\delta}$.

Recent studies have reported superconductivity in bilayer RP nickelate epitaxial thin films [9–11]. Although the experimental picture concerning the critical γ band remains contentious, thin-film samples exhibit a highly anisotropic $\mu_0 H_{c2}$ near T_c, following a quasi-2D behavior. The thickness of these films is typically around 2–3 unit cells, resulting in strong electron confinement within the a-b plane. In this context, when $H \parallel ab$, superconductivity is suppressed at the Clogston-Chandrasekhar limit. Consequently, $\mu_0 H_{c2}^{\parallel}$ of these thin-film samples displays a pronounced convex curvature near T_c, indicating strong Pauli paramagnetic effects. This significantly complicates the estimation of the intrinsic contribution of the d_{z^2} orbital. In contrast, when $H \perp ab$, orbital-limiting mechanisms become feasible. Notably, the $\mu_0 H_{c2}^{\perp}(T)$ in these thin films exhibits a quasilinear behavior [10,76], closely resembling our experimental results. It is instructive to compare pressurized $La_4Ni_3O_{10-\delta}$ with $La_3Ni_2O_{7-\delta}$. Unlike $La_4Ni_3O_{10-\delta}$, the superconducting transition of $La_3Ni_2O_{7-\delta}$ becomes broader with increasing magnetic field [2,3]. Such broadening, commonly associated with the formation of a vortex-liquid state, is frequently observed in superconductors with large anisotropic $\mu_0 H_{c2}$—including the cuprates and some iron-based SCs [77–79]. It implies that the $\mu_0 H_{c2}$ in $La_3Ni_2O_{7-\delta}$ is likely more anisotropic than in $La_4Ni_3O_{10-\delta}$. Nonetheless, direct investigation of the upper critical fields in pressurized $La_3Ni_2O_{7-\delta}$, particularly systematic studies of the relationship between its anisotropy and critical temperature, is crucial for understanding superconductivity in RP nickelates.

IV. CONCLUSION

In summary, by combining high-pressure and high-magnetic-field transport experiments, we have determined the complete temperature-magnetic-field phase diagram for the superconductor $La_4Ni_3O_{10-\delta}$. The upper critical field of $La_4Ni_3O_{10-\delta}$ is nearly isotropic across the entire temperature range, with the anisotropic parameter monotonically decreasing from about 1.4 near T_c toward unity at the lowest temperatures. Our analysis, based on the two-band model, suggests that the isotropic nature of $\mu_0 H_{c2}$ in $La_4Ni_3O_{10-\delta}$ arises from an effective balance between the anisotropic diffusivities of the bands contributed by d_{z^2} and $d_{x^2-y^2}$ orbitals. Our upper critical field studies provide evidence supporting the involvement of the d_{z^2} band in trilayer RP nickelates under pressure and highlight its crucial role in the emergence of superconductivity.

V. METHODS

A. Sample preparations

The precursor powder for the $La_4Ni_3O_{10-\delta}$ compound was prepared using the conventional solid-state reaction method. Single crystals were further grown using a vertical optical-image floating-zone furnace (model HKZ, SciDre). Details of the crystal growth procedure are given in Ref. [5]. To ensure consistency, all samples used in this study (sample S1–S5) were from the same batch.

B. Synchrotron x-ray single-crystal diffraction measurements

In situ high-pressure single-crystal synchrotron x-ray diffraction measurements were performed with a wavelength of 0.4834 Å at the beamline 17UM of Shanghai Synchrotron Radiation Facility, China. The measurements were carried out employing a symmetric diamond anvil cell with diamond culet sizes of approximately 300 μm and a rhenium gasket. The single-crystal sample was prepared by slicing it into a circular disk with a thickness of 6 μm and a diameter of 30 μm using FIB. The sample was then loaded into a sample chamber with a thickness of approximately 40 μm and a diameter of 180 μm drilled in the preindented rhenium gasket.

C. Measurements under high pressure

Measurements under pressure were carried out utilizing a DAC with 240 μm culets. The lamella was carved from a single crystal by using FIB milling and loaded with the *a-b* plane parallel to the diamond anvil culet of the DAC. For sample cutting, a gallium ion beam with a small beam current of 3 nA was employed to minimize damage. In all the high-pressure measurements conducted in this work, helium was employed as the pressure-transmitting medium to ensure optimal hydrostatic pressure conditions. Pressure calibration was accomplished by monitoring the shift of the fluorescence peak from ruby balls loaded along with the sample. The temperature dependence of the resistance was measured in a physical property measurement system (Quantum Design) and a He^4 cryostat in the high-magnetic-field facility. The dc magnetic susceptibility measurements under pressure were conducted using a custom-built beryllium-copper alloy miniature DAC. The measurements were performed using a magnetic property measurement system (MPMS3 Quantum Design).

D. Measurements under high magnetic fields

The high-field transport measurements up to 35 T were performed at the Chinese High Magnetic Field Laboratory at Hefei using a resistive water-cooled magnet (WM5). The DAC was mounted on the homemade spring-based rotator probe. The angle was determined by the Hall sensor fixed on the DAC. The resistivity was measured using the ac lock-in technique, where the current was generated by a current source (Keithely 6221), and the voltage was measured with a lock-in amplifier (SR 830).

ACKNOWLEDGMENTS

This work was supported by the National Key R&D Program of China (2021YFA0718900), the Shanghai Science and Technology Committee (Grant No. 22JC1410300), and Shanghai Key Laboratory of Material Frontiers Research in Extreme Environments (Grant No. 22dz2260800). This work at High Magnetic Field Laboratory was supported by the National Key R&D Program of the MOST of China (Grants No. 2022YFA1602602, No. 2024YFF0727900), the National Natural Science Foundation of China (Grant No. 12474053), the Basic Research Program of the Chinese Academy of Sciences Based on Major Scientific Infrastructures (Grant No. JZHKYPT-2021-08). We thank the WM5 [80] at the Steady High Magnetic Field Facility, CAS, for providing technical support and assistance in data collection and analysis. The work at Fudan University was supported by the Key Program of the National Natural Science Foundation of China (Grant No. 12234006), the National Key R&D Program of China (Grant No. 2022YFA1403202), the Innovation Program for Quantum Science and Technology (Grant No. 2024ZD0300103), and Shanghai Municipal Science and Technology Project (Grant No. 25DZ3008100). A portion of this research used resources at the beamline 17UM [81] of the Shanghai synchrotron radiation facility.

DATA AVAILABILITY

The data that support the findings of this article are not publicly available upon publication because it is not technically feasible and/or the cost of preparing, depositing, and hosting the data would be prohibitive within the terms of this research project. The data are available from the authors upon reasonable request.

[1] H. Sun, M. Huo, X. Hu, J. Li, Z. Liu, Y. Han *et al.*, *Signatures of superconductivity near 80 K in a nickelate under high pressure*, Nature (London) **621**, 493 (2023).

[2] Y. Zhang, D. Su, Y. Huang, Z. Shan, H. Sun, M. Huo *et al.*, *High-temperature superconductivity with zero resistance and strange-metal behaviour in* $La_3Ni_2O_{7-\delta}$, Nat. Phys. **20**, 1269 (2024).

[3] G. Wang, N. N. Wang, X. L. Shen, J. Hou, L. Ma, L. F. Shi *et al.*, *Pressure-induced superconductivity in polycrystalline* $La_3Ni_2O_{7-\delta}$, Phys. Rev. X **14**, 011040 (2024).

[4] Q. Li, Y.-J. Zhang, Z.-N. Xiang, Y. Zhang, X. Zhu, and H.-H. Wen, *Signature of superconductivity in pressurized* $La_4Ni_3O_{10-\delta}$, Chin. Phys. Lett. **41**, 017401 (2024).

[5] Y. Zhu, D. Peng, E. Zhang, B. Pan, X. Chen, L. Chen *et al.*, *Superconductivity in pressurized trilayer* $La_4Ni_3O_{10-\delta}$ *single crystals*, Nature (London) **631**, 531 (2024).
[6] M. Zhang, C. Pei, D. Peng, X. Du, W. Hu, Y. Cao *et al.*, *Superconductivity in trilayer nickelate* $La_4Ni_3O_{10-\delta}$ *under pressure*, Phys. Rev. X **15**, 021005 (2025).
[7] N. Wang, G. Wang, X. Shen, J. Hou, J. Luo, X. Ma *et al.*, *Bulk high-temperature superconductivity in pressurized tetragonal* $La_2PrNi_2O_{7-\delta}$, Nature (London) **634**, 579 (2024).
[8] Y. Zhou, J. Guo, S. Cai, H. Sun, C. Li, J. Zhao *et al.*, *Investigations of key issues on the reproducibility of high-*T_c *superconductivity emerging from compressed* $La_3Ni_2O_{7-\delta}$, Matter Radiat. Extremes **10**, 027801 (2025).
[9] E. K. Ko, Y. Yu, Y. Liu, L. Bhatt, J. Li, V. Thampy *et al.*, *Signatures of ambient pressure superconductivity in thin film* $La_3Ni_2O_{7-\delta}$, Nature (London) **638**, 935 (2025).
[10] G. Zhou, W. Lv, H. Wang, Z. Nie, Y. Chen, Y. Li *et al.*, *Ambient-pressure superconductivity onset above 40 K in* $(La,Pr)_3Ni_2O_7$ *films*, Nature (London) **640**, 641 (2025).
[11] Y. Liu, E. K. Ko, Y. Tarn, L. Bhatt, J. Li, V. Thampy *et al.*, *Superconductivity and normal-state transport in compressively strained* $La_2PrNi_2O_{7-\delta}$ *thin films*, Nat. Mater. **24**, 1221 (2025).
[12] Z. Luo, X. Hu, M. Wang, W. Wu, and D.-X. Yao, *Bilayer two-orbital model of* $La_3Ni_2O_{7-\delta}$ *under pressure*, Phys. Rev. Lett. **131**, 126001 (2023).
[13] Y. Gu, C. Le, Z. Yang, X. Wu, and J. Hu, *Effective model and pairing tendency in the bilayer Ni-based superconductor* $La_3Ni_2O_{7-\delta}$, Phys. Rev. B **111**, 174506 (2025).
[14] V. Christiansson, F. Petocchi, and P. Werner, *Correlated electronic structure of* $La_3Ni_2O_{7-\delta}$ *under pressure*, Phys. Rev. Lett. **131**, 206501 (2023).
[15] Y. Cao and Y. F. Yang, *Flat bands promoted by Hund's rule coupling in the candidate double-layer high-temperature superconductor* $La_3Ni_2O_{7-\delta}$ *under high pressure*, Phys. Rev. B **109**, L081105 (2024).
[16] Y.-B. Liu, J.-W. Mei, F. Ye, W.-Q. Chen, and F. Yang, *s-wave pairing and the destructive role of apical-oxygen deficiencies in* $La_3Ni_2O_{7-\delta}$ *under pressure*, Phys. Rev. Lett. **131**, 236002 (2023).
[17] X.-Z. Qu, D.-W. Qu, J. Chen, C. Wu, F. Yang, W. Li, and G. Su, *Bilayer* $t-J-J_\perp$ *model and magnetically mediated pairing in the pressurized nickelate* $La_3Ni_2O_{7-\delta}$, Phys. Rev. Lett. **132**, 036502 (2024).
[18] Y. F. Yang, G.-M. Zhang, and F.-C. Zhang, *Interlayer valence bonds and two-component theory for high-*T_c *superconductivity of* $La_3Ni_2O_{7-\delta}$ *under pressure*, Phys. Rev. B **108**, L201108 (2023).
[19] Q. Qin and Y. F. Yang, *High-*T_c *superconductivity by mobilizing local spin singlets and possible route to higher* T_c *in pressurized* $La_3Ni_2O_{7-\delta}$, Phys. Rev. B **108**, L140504 (2023).
[20] J.-X. Wang, Z. Ouyang, R.-Q. He, and Z.-Y. Lu, *Non-Fermi liquid and Hund correlation in* $La_4Ni_3O_{10-\delta}$ *under high pressure*, Phys. Rev. B **109**, 165140 (2024).
[21] C. Lu, Z. Pan, F. Yang, and C. Wu, *Superconductivity in* $La_4Ni_3O_{10-\delta}$ *under pressure*, Phys. Rev. B **111**, 134515 (2025).
[22] C.-Q. Chen, Z. Luo, M. Wang, W. W, and D.-X. Yao, *Trilayer multiorbital models of* $La_4Ni_3O_{10-\delta}$, Phys. Rev. B **110**, 014503 (2024).
[23] M. Zhang, H. Sun, Y.-B. Liu, Q. Liu, W.-Q. Chen, and F. Yang, $s^{\pm}$*-wave superconductivity in pressurized* $La_4Ni_3O_{10-\delta}$, Phys. Rev. B **110**, L180501 (2024).
[24] C. Lu, Z. Pan, F. Yang, and C. Wu, *Interlayer-coupling-driven high-temperature superconductivity in* $La_3Ni_2O_{7-\delta}$ *under pressure*, Phys. Rev. Lett. **132**, 146002 (2024).
[25] W. W, Z. Luo, D.-X. Yao, and M. Wang, *Superexchange and charge transfer in the nickelate superconductor* $La_3Ni_2O_{7-\delta}$ *under pressure*, Sci. China Phys. Mech. Astron. **67**, 117402 (2024).
[26] J. Zhan, Y. Gu, X. Wu, and J. Hu, *Cooperation between electron-phonon coupling and electronic interaction in bilayer nickelates* $La_3Ni_2O_{7-\delta}$, Phys. Rev. Lett. **134**, 136002 (2025).
[27] Z. Huo, Z. Luo, P. Zhang, A. Yang, Z. Liu, X. Tao *et al.*, *Modulation of the octahedral structure and potential superconductivity of* $La_3Ni_2O_{7-\delta}$ *through strain engineering*, Sci. China Phys. Mech. Astron. **68**, 237411 (2025).
[28] Z. Ouyang, R.-Q. He, and Z.-Y. Lu, *Phase diagrams and two key factors to superconductivity of Ruddlesden-Popper nickelates*, Phys. Rev. B **112**, 045127 (2025).
[29] Y.-Q. Liu, D. Wang, and Q.-H. Wang, *Variational quantum Monte Carlo investigations of the superconducting pairing in* $La_3Ni_2O_{7-\delta}$, Phys. Rev. B **112**, 014511 (2025).
[30] F. Lechermann, J. Gondolf, S. Btzel, and I. M. Eremin, *Electronic correlations and superconducting instability in* $La_3Ni_2O_{7-\delta}$ *under high pressure*, Phys. Rev. B **108**, L201121 (2023).
[31] K. Jiang, Z. Wang, and F.-C. Zhang, *High-temperature superconductivity in* $La_3Ni_2O_{7-\delta}$, Chin. Phys. Lett. **41**, 017402 (2024).
[32] Y.-H. Tian, Y. Chen, J.-M. Wang, R.-Q. He, and Z.-Y. Lu, *Correlation effects and concomitant two-orbital* $s_{\pm}$*-wave superconductivity in* $La_3Ni_2O_{7-\delta}$ *under high pressure*, Phys. Rev. B **109**, 165154 (2024).
[33] J.-X. Zhang, H.-K. Zhang, Y.-Z. You, and Z.-Y. Weng, *Strong pairing originated from an emergent* $\mathbb{Z}_2$ *Berry phase in* $La_3Ni_2O_{7-\delta}$, Phys. Rev. Lett. **133**, 126501 (2024).
[34] H. LaBollita, V. Pardo, M. R. Norman, and A. S. Botana, *Electronic structure and magnetic properties of* $La_3Ni_2O_{7-\delta}$ *under pressure: Active role of the* $Ni-d_{x^2-y^2}$ *orbitals*, arXiv:2309.17279.
[35] C. Xia, H. Liu, S. Zhou, and H. Chen, *Sensitive dependence of pairing symmetry on Ni-*e_g *crystal field splitting in the nickelate superconductor* $La_3Ni_2O_{7-\delta}$, Nat. Commun. **16**, 1054 (2025).
[36] Z. Fan, J.-F. Zhang, B. Zhan, D. Lv, X.-Y. Jiang, B. Normand, and T. Xiang, *Superconductivity in nickelate and cuprate superconductors with strong bilayer coupling*, Phys. Rev. B **110**, 024514 (2024).
[37] I. V. Leonov, *Electronic structure and magnetic correlations in the trilayer nickelate superconductor* $La_4Ni_3O_{10-\delta}$ *under pressure*, Phys. Rev. B **109**, 235123 (2024).
[38] H. LaBollita, J. Kapeghian, M. R. Norman, and A. S. Botana, *Electronic structure and magnetic tendencies of trilayer* $La_4Ni_3O_{10-\delta}$ *under pressure: Structural transition, molecular orbitals, and layer differentiation*, Phys. Rev. B **109**, 195151 (2024).
[39] L. B. Braz, G. B. Martins, and Luis G. G. V. Dias da Silva, *Interlayer interactions in* $La_3Ni_2O_{7-\delta}$ *under pressure: From*

$s^{\pm}$ *to* d_{xy}*-wave superconductivity*, Phys. Rev. Res. **7**, 033023 (2025).

[40] C. Chen, C. Chen, K. Li, X. Sui, W. Long, H. Yang, and B. Huang, *Enhancement of dominant* d_{xy}*-wave pairing in the overdoped Hubbard model with next-nearest hopping* t', Phys. Rev. B **112**, 115148 (2025).

[41] Q.-G. Yang, D. Wang, and Q.-H. Wang, *Possible* $s_{\pm}$*-wave superconductivity in* $La_3Ni_2O_{7-\delta}$, Phys. Rev. B **108**, L140505 (2023).

[42] H. Sakakibara, N. Kitamine, M. Ochi, and K. Kuroki, *Possible high* T_c *superconductivity in* $La_3Ni_2O_{7-\delta}$ *under high pressure through manifestation of a nearly half-filled bilayer Hubbard model*, Phys. Rev. Lett. **132**, 106002 (2024).

[43] Y. Zhang, L.-F. Lin, A. Moreo, T. A. Maier, and E. Dagotto, *Trends in electronic structures and* $s_{\pm}$*-wave pairing for the rare-earth series in bilayer nickelate superconductor* $R_3Ni_2O_{7-\delta}$, Phys. Rev. B **108**, 165141 (2023).

[44] J. Huang, Z. D. Wang, and T. Zhou, *Impurity and vortex states in the bilayer high-temperature superconductor* $La_3Ni_2O_{7-\delta}$, Phys. Rev. B **108**, 174501 (2023).

[45] H. Oh and Y.-H. Zhang, *Type-II* $t-J$ *model and shared superexchange coupling from Hunds rule in superconducting* $La_3Ni_2O_{7-\delta}$, Phys. Rev. B **108**, 174511 (2023).

[46] Y. Zhang, L.-F. Lin, A. Moreo, T. A. Maier, and E. Dagotto, *Prediction of* $s^{\pm}$*-wave superconductivity enhanced by electronic doping in trilayer nickelates* $La_4Ni_3O_{10-\delta}$ *under pressure*, Phys. Rev. Lett. **133**, 136001 (2024).

[47] Y. Zhang, L.-F. Lin, A. Moreo, T. A. Maier, and E. Dagotto, *Structural phase transition, s-wave pairing, and magnetic stripe order in bilayered superconductor* $La_3Ni_2O_{7-\delta}$ *under pressure*, Nat. Commun. **15**, 2470 (2024).

[48] K.-Y. Jiang, Y.-H. Cao, Q.-G. Yang, H.-Y. Lu, and Q.-H. Wang, *Theory of pressure dependence of superconductivity in bilayer nickelate* $La_3Ni_2O_{7-\delta}$, Phys. Rev. Lett. **134**, 076001 (2025).

[49] P. Borchia, H. Lange, and F. Grusdt, *Extended s-wave pairing from an emergent feshbach resonance in bilayer nickelate superconductors*, Phys. Rev. B **112**, 165143 (2025).

[50] Y. Zhang, L.-F. Lin, A. Moreo, and E. Dagotto, *Electronic structure, dimer physics, orbital-selective behavior, and magnetic tendencies in the bilayer nickelate superconductor* $La_3Ni_2O_{7-\delta}$ *under pressure*, Phys. Rev. B **108**, L180510 (2023).

[51] Z. Liao, L. Chen, G. Duan, Y. Wang, C. Liu, R. Yu, and Q. Si, *Electron correlations and superconductivity in* $La_3Ni_2O_{7-\delta}$ *under pressure tuning*, Phys. Rev. B **108**, 214522 (2023).

[52] R. Jiang, J. Hou, Z. Fan, Z.-J. Lang, and W. Ku, *Pressure driven fractionalization of ionic spins results in cupratelike high-*T_c *superconductivity in* $La_3Ni_2O_{7-\delta}$, Phys. Rev. Lett. **132**, 126503 (2024).

[53] Z. Luo, B. Lv, M. Wang, W. W, and D.-X. Yao, *High-*T_c *superconductivity in* $La_3Ni_2O_{7-\delta}$ *based on the bilayer two-orbital t-J model*, npj Quantum Mater. **9**, 61 (2024).

[54] S. Ryee, N. Witt, and T. O. Wehling, *Quenched pair breaking by interlayer correlations as a key to superconductivity in* $La_3Ni_2O_{7-\delta}$, Phys. Rev. Lett. **133**, 096002 (2024).

[55] G. Heier, K. Park, and S. Y. Savrasov, *Competing* d_{xy} *and* $s_{\pm}$ *pairing symmetries in superconducting* $La_3Ni_2O_{7-\delta}$*: LDA + FLEX calculations*, Phys. Rev. B **109**, 104508 (2024).

[56] T. T. M. Palstra, B. Batlogg, L. F. Schneemeyer, R. B. van Dover, and J. V. Waszczak, *Angular dependence of the upper critical field of* $Bi_{2.2}Sr_2Ca_{0.8}Cu_2O_{8+\delta}$, Phys. Rev. B **38**, 5102 (1988).

[57] M. J. Naughton, R. C. Yu, P. K. Davies, J. E. Fischer, R. V. Chamberlin, Z. Z. Wang, T. W. Jing, N. P. Ong, and P. M. Chaikin, *Orientational anisotropy of the upper critical field in single-crystal* $YBa_2Cu_3O_7$ *and* $Bi_{2.2}CaSr_{1.9}Cu_2O_{8+x}$, Phys. Rev. B **38**, 9280 (1988).

[58] F. Hunte, J. Jaroszynski, A. Gurevich, D. C. Larbalestier, R. Jin, A. S. Sefat, M. A. McGuire, B. C. Sales, D. K. Christen, and D. Mandrus, *Two-band superconductivity in* $LaFeAsO_{0.89}F_{0.11}$ *at very high magnetic fields*, Nature (London) **453**, 903 (2008).

[59] H. Q. Yuan, J. Singleton, F. F. Balakirev, S. A. Baily, G. F. Chen, J. L. Luo, and N. L. Wang, *Nearly isotropic superconductivity in* $(Ba,K)Fe_2As_2$, Nature (London) **457**, 565 (2009).

[60] See Supplemental Material at http://link.aps.org/supplemental/10.1103/h5sv-dzd1 for additional information about sample characterization, the repeatability of the experiment, two-band model fitting, and the angle dependence of the T_c.

[61] R. A. Cooper, Y. Wang, B. Vignolle, O. J. Lipscombe, S. M. Hayden, Y. Tanabe *et al.*, *Anomalous criticality in the electrical resistivity of* $La_{2-x}Sr_xCuO_4$, Science **323**, 603 (2009).

[62] J. Yuan, Q. Chen, K. Jiang, Z. Feng, Z. Lin, H. Yu *et al.*, *Scaling of the strange-metal scattering in unconventional superconductors*, Nature (London) **602**, 431 (2022).

[63] S. Licciardello, J. Buhot, J. Lu, J. Ayres, S. Kasahara, Y. Matsuda, T. Shibauchi, and N. E. Hussey, *Electrical resistivity across a nematic quantum critical point*, Nature (London) **567**, 213 (2019).

[64] X. Jiang, M. Qin, X. Wei, L. Xu, J. Ke, H. Zhu *et al.*, *Interplay between superconductivity and the strange-metal state in* FeSe, Nat. Phys. **19**, 365 (2023).

[65] K. Lee, B. Y. Wang, M. Osada, B. H. Goodge, T. C. Wang, Y. Lee *et al.*, *Linear-in-temperature resistivity for optimally superconducting* $(Nd,Sr)NiO_2$, Nature (London) **619**, 288 (2023).

[66] N. R. Werthamer, E. Helfand, and P. C. Hohenberg, *Temperature and purity dependence of the superconducting critical field,* H_{c2}*. III. Electron spin and spin-orbit effects*, Phys. Rev. **147**, 295 (1966).

[67] A. M. Clogston, *Upper limit for the critical field in hard superconductors*, Phys. Rev. Lett. **9**, 266 (1962).

[68] D. Li, K. Lee, B. Y. Wang, M. Osada, S. Crossley, H. R. Lee, Y. Cui, Y. Hikita, and H. Y. Hwang, *Superconductivity in an infinite-layer nickelate*, Nature (London) **572**, 624 (2019).

[69] B. Y. Wang, D. Li, B. H. Goodge, K. Lee, M. Osada, S. P. Harvey, L. F. Kourkoutis, M. R. Beasley, and H. Y. Hwang, *Isotropic Pauli-limited superconductivity in the infinite-layer nickelate* $Nd_{0.775}Sr_{0.225}NiO_2$, Nat. Phys. **17**, 473 (2021).

[70] B. Y. Wang, T. C. Wang, Y.-T. Hsu, M. Osada, K. Lee, C. Jia *et al.*, *Effects of rare-earth magnetism on the superconducting upper critical field in infinite-layer nickelates*, Sci. Adv. **9**, eadf6655 (2023).

[71] A. Gurevich, *Enhancement of the upper critical field by nonmagnetic impurities in dirty two-gap superconductors*, Phys. Rev. B **67**, 184515 (2003).

[72] A. Gurevich, *Iron-based superconductors at high magnetic fields*, Rep. Prog. Phys. **74**, 124501 (2011).

[73] D. R. Tilley, *The Ginsburg-Landau equations for anisotropic alloys*, Proc. Phys. Soc. London **86**, 289 (1965).

[74] G. Blatter, V. B. Geshkenbein, and A. I. Larkin, *From isotropic to anisotropic superconductors: A scaling approach*, Phys. Rev. Lett. **68**, 875 (1992).

[75] U. Welp, W. K. Kwok, G. W. Crabtree, K. G. Vandervoort, and J. Z. Liu, *Angular dependence of the upper critical field of* $YBa_2Cu_3O_{7-\delta}$ *single crystals*, Phys. Rev. B **40**, 5263 (1989).

[76] Y.-T. Hsu, Y. Liu, Y. Kohama, T. Kotte, V. Sharma, Y. Tarn, Y. Yu, and H. Y. Hwang, *Fermi-liquid transport beyond the upper critical field in superconducting* $La_2PrNi_2O_7$ *thin films*, arXiv:2505.19011.

[77] T. T. M. Palstra, B. Batlogg, R. B. van Dover, L. F. Schneemeyer, and J. V. Waszczak, *Dissipative flux motion in high-temperature superconductors*, Phys. Rev. B **41**, 6621 (1990).

[78] J. Jaroszynski, F. Hunte, L. Balicas, Y. J. Jo, I. Raievi, A. Gurevich, D. C. Larbalestier, F. F. Balakirev, L. Fang, P. Cheng, Y. Jia, and H. H. Wen, *Upper critical fields and thermally-activated transport of* $NdFeAsO_{0.7}F_{0.3}$ *single crystal*, Phys. Rev. B **78**, 174523 (2008).

[79] L. Jiao, Y. Kohama, J. L. Zhang, H. D. Wang, B. Maiorov, F. F. Balakirev *et al.*, *Upper Critical field and thermally activated flux flow in single-crystalline* $Tl_{0.58}Rb_{0.42}Fe_{1.72}Se_2$, Phys. Rev. B **85**, 064513 (2012).

[80] https://cstr.cn/31125.02.SHMFF.WM5.

[81] https://cstr.cn/31124.02.SSRF.BL17UM.